Computational and Structural Biotechnology Journal 19 (2021) 2477–2485

COMPUTATIONAL AND STRUCTURAL BIOTECHNOLOGY JOURNAL

journal homepage: www.elsevier.com/locate/csbj

In vivo genome editing in single mammalian brain neurons through CRISPR-Cas9 and cytosine base editors

Beomjong Song [a,1,*], Chan Young Kang [b,1], Jun Hee Han [b], Masanobu Kano [a,c], Arthur Konnerth [a,d,e], Sangsu Bae [b,2,*]

[a] International Research Center for Neurointelligence (WPI-IRCN), The University of Tokyo, Hongo, Bunkyo-ku, Tokyo 113-0033, Japan
[b] Department of Chemistry and Research Institute for Convergence of Basic Sciences, Hanyang University, Seoul 04763, South Korea
[c] Department of Neurophysiology, Graduate School of Medicine, The University of Tokyo, Tokyo 113-0033, Japan
[d] Institute of Neuroscience, Technical University of Munich, 80802 Munich, Germany
[e] Munich Cluster for Systems Neurology, Technical University of Munich, 80802 Munich, Germany

ARTICLE INFO

Article history:
Received 11 January 2021
Received in revised form 20 April 2021
Accepted 22 April 2021
Available online 25 April 2021

Keywords:
CRISPR-Cas9
Base editors
In vivo targeted single-cell electroporation
Neuron
Brain

ABSTRACT

Gene manipulation is a useful approach for understanding functions of genes and is important for investigating basic mechanisms of brain function on the level of single neurons and circuits. Despite the development and the wide range of applications of CRISPR-Cas9 and base editors (BEs), their implementation for an analysis of individual neurons *in vivo* remained limited. In fact, conventional gene manipulations are generally achieved only on the population level. Here, we combined either CRISPR-Cas9 or BEs with the targeted single-cell electroporation technique as a proof-of-concept test for gene manipulation in single neurons *in vivo*. Our assay consisted of CRISPR-Cas9- or BEs-induced gene knockout in single Purkinje cells in the cerebellum. Our results demonstrate the feasibility of both gene editing and base editing in single cells in the intact brain, providing a tool through which molecular perturbations of individual neurons can be used for analysis of circuits and, ultimately, behaviors.

1. Introduction

The remarkable expansion of our knowledge about the brain has is indebted to research exploring how specific molecules related to cellular activities underlie high-dimensional and complex brain functions such as perception, prediction, attention, and learning. Thus, many studies investigated the roles of relevant genes in neural circuits by assessing effects of gene manipulation such as gene overexpression, knock-in, or knockout. Especially, gene knockout is a direct way to reveal the roles of a gene, and the development of transgenic animals has been a typical strategy exploiting gene knockout [1–3]. However, this approach has potential limitations including i) the complete knockout of some genes, especially those that are essential or associated with early development can be lethal, thus the production of knockout animals for those genes is extremely difficult, ii) the characteristics of some genes may be diverse, depending on developmental stage and/or cell type, and iii) the functional loss of a specific genes may be compensated by other genes during development.

To overcome these limitations, several conditional knockout methods were developed, in which a gene of interest can be knocked out in a specific cell type at desired time points [4]. This approach exploits DNA recombinases such as Cre or FLP and recombinase recognition target sites such as loxP or FRT respectively in concert. These are typically placed in the introns flanking the target gene [5]. The target gene knockout can be controlled by the expression of the DNA recombinase [6–8]. However, this strategy fundamentally requires the construction of transgenic animals containing the recombinase system. Furthermore, single nucleotide conversion in a gene is not easy with this system.

In recent years, the emergence of the CRISPR-Cas9 system revolutionized targeted gene editing at the gene of interest [9–11]. Researchers can now easily disrupt or regulate a specific gene in a target organism such as the brain *in vivo* simply by delivering the CRISPR system into the target region [12–18]. In addition to the CRISPR nucleases, DNA base editors (BEs) including cytosine base editor (CBE) [19,20] and adenine base editor (ABE) [21] were recently developed, enabling single nucleotide conversion without

* Corresponding authors.
E-mail addresses: b_song@m.u-tokyo.ac.jp (B. Song), sangsubae@hanyang.ac.kr (S. Bae).
[1] These authors contributed equally to this work.
[2] Lead contact

https://doi.org/10.1016/j.csbj.2021.04.051

generating double strand breaks (DSBs) in the target DNA, so that they can complement the drawbacks of the use of CRISPR nucleases.

Until now, CRISPR nucleases and BEs have been widely harnessed in various organs or tissues of animals *in vivo*, but targeted gene editing in a single cell has not yet been reported. Here, we demonstrate gene editing and base editing in a single Purkinje cell in the cerebellum of mice by respectively transfecting a Cas9 nuclease or a CBE via targeted single-cell electroporation *in vivo* [22,23], possibly enabling the genetic perturbation to a single cell within a neural circuit in the intact brain.

2. Materials and methods

2.1. Animals

All experiments were performed in accordance with the guidelines set down by the experimental animal ethics committees of The University of Tokyo. 2 to 4.5 month-old L7-enhanced green fluorescent protein (EGFP) transgenic mice were used [24].

2.2. sgRNA design and gene editing efficiency test

Five sgRNAs were designed to respectively target parts of the EGFP sequence using Cas-designer [25]. For sgRNA cloning, pRG2 was used. pRG2 and p3s-Cas9-HN were gifts from Jin-Soo Kim (Addgene plasmid #104174, Addgene plasmid #104171), and pCMV_AncBE4max was a gift from David Liu (Addgene plasmid # 112094). Especially, sgRNA#5 was designed to make C > T conversion of 184th and 185th Glutamine (CAG) by CBE (AncBE4max) to introduce premature stop codon (TAG). The sgRNAs were designed in 20 ~ 80% CDS region of EGFP. For *in vitro* test of the gene editing efficiency, HEK 293T cells expressing EGFP were grown in DMEM with 10% FBS and 1% antibiotic antimycotic solution (10,000 units/ml penicillin, 10 mg/ml streptomycin sulfate and 25 ug/ml amphotericin B). *Sp*Cas9 plasmid (150 ng) and each sgRNA plasmid (50 ng) were co-transfected into 1×10^5 HEK 293T-EGFP cells using Neon Transfection system (Invitrogen) with a single pulse (voltage: 1100 V; pulse duration: 40 ms), and they were seeded into a 24-well plate (Corning, 3524). 72 hrs after the transfection, genomic DNA of the transfected HEK 293T-EGFP cells was lysed using buffer composed of 40 mM Tris (pH 8.0), 1% Tween-20, 0.2% Nonidet P-40, 0.2 mM EDTA, and 40 μg/ml proteinase at 60C for 15 min followed by boiling at 98C for 5 min.

2.3. Construction of EGFP knock-in human cells

DNA sequences encoding EGFP gene were integrated into the C-terminus of the coactivator associated arginine methyltransferase 1 (CARM1) gene through a CRISPR-mediated homology direct repair (HDR) method in HEK 293T cells. EGFP was stably expressed under the endogenous CARM1 promoter. For the cell line construction, 1×10^5 HEK 293T cells were seeded in a 24-well plate. 250 ng gRNA plasmid, 750 ng Cas9 plasmid, and 500 ng HDR donor plasmid were delivered using lipofectamine 2000. Cells with 1% highly ranked EGFP signal were sorted by a flow cytometry and then seeded to a 96-well plate as a single cell. After construction of CARM1-EGFP single cell line, EGFP sequence was confirmed through Sanger sequencing.

2.4. Targeted deep sequencing

For EGFP gene sequencing, each EGFP gene locus targeted by the sgRNAs was amplified by nested PCR using Multi & Epi (TOYOBO) with forward/reverse primers (Table S1). PCR amplicons were sequenced with Miniseq (Illumina). After sequencing, Fastq-join files were analyzed using Cas-analyzer (http://www.rgenome.net/-cas-analyzer/) [26] for measuring insertion and deletion frequency. Rare sequence reads ($\leq$1) were excluded. For testing the gene editing efficiency of CBE (AncBE4max), AncBE4max plasmid (150 ng) and sgRNA#5 plasmid (50 ng) were co-transfected into HEK 293T-EGFP cells. Then NGS sampling was performed in the same way, and the editing efficiency was analyzed by BE-analyzer (http://www.rgenome.net/be-analyzer/) [27].

2.5. Gibson assembly

Gibson assembly was performed as previously described [28]. pRG2 was cleaved with *in vitro* cleavage, using $sgRNA^{(F+E)}$ and SpCas9 protein. The $sgRNA^{(F+E)}$ is a structurally optimized form by combining the A-U flip and hairpin extension, which showed improved editing activity [29]. The mCherry cassette was amplified and inserted into pRG2 backbone by Gibson assembly (Table S1). The plasmids were confirmed with Sanger sequencing.

2.6. Surgery

For two-photon imaging and single-cell electroporation, a cranial window was made over vermis VI of the cerebellum. Anesthesia was induced with 2% isoflurane (Pfizer Japan, Tokyo) in air and maintained at a level of 0.7% during surgery, electroporation, and imaging. The body temperature was continuously monitored and maintained by a heated pad at 38 °C. Both eyes were covered with ophthalmic ointment. Dexamethasone sodium phosphate (4.8 mg/kg) was subcutaneously injected 1–2 hrs before craniotomy to prevent inflammation. To fix an animal head during the electroporation and the two-photon imaging, a head plate made of carbon fiber was implanted on the skull using Optibond (Kerr) and Tetric N-Flow (Ivoclar Vivadent) after injecting a local anesthetic (1% xylocaine) and an analgesic (flunixin meglumine, 2.5 mg/kg). The plastic chamber for applying artificial cerebrospinal fluid (aCSF) was attached on it. Then a rectangle cranial window (3 mm × 2 mm) was made over the cerebellar vermis VI using a dental drill. 2% agarose dissolved in saline was applied to the cranial window before targeted single-cell electroporation to minimize brain movement.

2.7. Two-photon microscopy

Two-photon imaging was performed with a custom-built microscope [30]. The microscope was equipped with a 12-kHz resonant scanner (Cambridge Technology) and controlled by LabVIEW. The excitation laser was a mode-locked Ti:sapphire laser (Chameleon Discovery, Coherent) for EGFP imaging (920 nm) and a fiber laser (Fidelity-2, Coherent) for Alexa594 or mCherry imaging (1070 nm). Their light paths were merged with a polarizing beamsplitter cube (CM05-PBS203, Thorlabs), but their output power was independently controlled by a Pockels cell (Conopotics) and by an acousto-optic deflector (AA OPTO-ELECTRONIC), respectively. The laser power just below the microscope objective (40 × NA 0.8, Nikon) was 20–35 mW (920 nm) and 5–30 mW (1070 nm) for imaging. The emitted fluorescence signals of EGFP and mCherry were detected by each photomultiplier tube (H7422-40, Hamamatsu) after being filtered by a beamsplitter (T 565 SPXR, AHF analysentechnik AG). The EGFP and mCherry fluorescence signals in the electroporated cells were measured every day for 3–4 weeks. For this, the animals were anesthetized with 0.7% isoflurane, and the animal heads were fixed to the imaging table through the head plate. Imaging of each cell was done in 180 μm × 180 μm sized area for 15 secs at 40 Hz sampling rate.

2.8. In vivo targeted single-cell electroporation and glass implantation

Targeted single-cell electroporation of DNA plasmids was performed under two-photon visual guidance [22,23]. A pipette (resistance of 7–10 MΩ) was loaded with a pipette solution (135 mM K-gluconate, 4 mM KCl, 10 mM HEPES, 4 mM Mg-ATP, 0.3 mM Na_2-GTP, and 10 mM-Phosphocreatine) containing DNA plasmids (Cas9, 400–600 ng/μl; sgRNA#4, 200–300 ng/μl; AncBE4-max, 300–500 ng/μl; sgRNA#5, 200–300 ng/μl). Because EGFP was expressed in Purkinje cells in L7-EGFP mice, Alexa 594 (50 μM) was also included in the pipette solution to visualize the glass pipette in the brain without being blurred by EGFP fluorescence from Purkinje cells. The brain surface was soaked with HEPES-based aCSF (145 mM NaCl, 5 mM KCl, 2 mM $CaCl_2$, 1 mM $MgCl_2$, 10 mM HEPES; 300 mOsm; pH 7.4 adjusted with NaOH). Once confirmed that the physical contact between the glass pipette and the target cell was formed properly by monitoring the shadow of the cell generated by the ejected Alex 594 dye [22], an electrical pulse train (pulse amplitude, −6 V; width, 1.2 s; duration, 0.2 ms; interpulse interval, 10 ms) was applied 3 times through the amplifier (ELC-03XS, NPI). It was confirmed whether the targeted cell was actually electroporated, by checking the fluorescence signal of Alex 594 dye in the target cell after the electroporation. Then, the glass pipette was retracted carefully. After several trials of the electroporation, the cranial window was covered with a glass (No.1, Matsunami) trimmed to make a rectangle (3 mm × 2 mm), and dental adhesive resin cement (Superbond, Sun Medical) was applied to fix the cover glass. The mice were kept alive for 3–4 weeks for monitoring the fluorescence serially.

2.9. Data analysis

Data were analyzed using MATLAB (MathWorks) and Graphpad Prism (GraphPad software, USA), and the images were processed using ImageJ [31]. Statistical tests were described in the main text and the figure legends. All statistical tests were two-sided (*p < 0.05, **p < 0.01, ***p < 0.001, ****p < 0.0001). A parametric statistical test (Student's *t*-test) was used after confirming that the data set passed the Shapiro-Wilk normality test. Data were displayed as mean ± standard error of the mean (SEM). Quantification of the EGFP fluorescence signal was performed as follows: The EGFP fluorescence signal of a target cell was divided by those of 3–4 neighboring cells and then averaged to obtain relative EGFP fluorescence signal intensity. In order to measure the change in EGFP fluorescence signal over time, the relative EGFP fluorescence signal intensity of each day was normalized to that on Day 2.

3. Results

3.1. Establishment of a single cell targeting system in L7-EGFP mice

To demonstrate single-cell editing *in vivo*, we prepared transgenic mice, named L7-EGFP [24], of which EGFP genes with a mouse Purkinje cell protein 2 promoter (or L7-1 promoter) were integrated in the genome. Hence, the L7-EGFP mice show highly specific EGFP expression in Purkinje cells of the cerebellum. For *in vivo* EGFP gene targeting, we used either CRISPR-Cas9 or CBE tools with a dual-plasmid system; one encoding either Cas9 or CBE, and the other encoding single-guide RNAs (sgRNAs) with a red fluorescence protein (mCherry) gene to confirm the plasmid transfection into a target cell as well as the survival of the cell after transfection throughout the experiment (Fig. 1). Therefore, Cas9 or CBE components-transfected Purkinje cells will exhibit a red fluorescence signal together with the green signal, whereas non-transfected Purkinje cells in L7-EGFP mice will exhibit green fluorescence only. If the EGFP gene is successfully knocked out, the green fluorescence will dissipate in the plasmid-transfected cells, while the red fluorescence signal remains. For transfection of the plasmids, we employed *in vivo* targeted single-cell electroporation [22,23] with modified parameters (Fig. 1). The two kinds of plasmid can be injected at once by electroporation at the single-cell level, and the fluorescence signals can be detected by a two-photon microscope *in vivo*.

3.2. Cas9 nuclease-mediated endogenous EGFP knockout in a single Purkinje cell

We first performed *in vivo* EGFP gene knockout experiments in a single cell via CRISPR-Cas9. The Cas9 nucleases can generate guide RNA-specific DNA cleavages in cells and the non-homologous end joining (NHEJ) repair pathway frequently leads to small nucleotide insertions and deletions (indels) at the cleavage site, resulting in frameshift-mediated gene knockout (Fig. 2A). To this end, we designed five sgRNAs for targeting the functional domain (amino acids 7–229) of EGFP gene which is crucial for EGFP fluorescence [32] and selected sgRNA#4 arbitrarily because all the five sgRNAs showed high indel-induction capabilities (>85%) in a human cell system (Fig. S1). Then, we electroporated the CRISPR-Cas9 components encoded in the dual plasmids (i.e., one for Cas9 and the other for sgRNA#4/mCherry) into Purkinje cells *in vivo*, for the EGFP gene knockout. We also transfected the sgRNA#4/mCherry-encoding plasmid alone as a negative control.

In this experiment, we electroporated 46 Purkinje neurons in 7 animals and about half of them (25 cells) showed mCherry expression. The success rate (54%) of our study done in the cerebellum was relatively lower than the rates of previous studies performed in the cerebral cortex (70 ~ 75%) [22,23], which might be due to the compactness of the cerebellum. The cerebellum is essentially packed with numerous cells, and this often hinders physical contact between a glass pipette and target cell membrane or blocks the opening of the glass pipette, thereby possibly preventing efficient delivery of plasmids into the cells via electroporation. Among the 25 mCherry-expressing cells, 16 cells (10 cells, Cas9 + sgRNA#4; 6 cells, sgRNA#4) survived throughout the experiment (for 3 weeks). We found that mCherry fluorescence appeared within 1–3 days after electroporation (Fig. 2B), indicating that plasmids were successfully delivered into the target neurons. Although the mCherry fluorescence signal was observed for 20 days, its intensity became weaker as time passed by. Because mCherry gene did not contain any potential target sites of the sgRNAs designed for targeting EGFP gene, it is unlikely that mCherry expression became weaker by the activities of CRISPR-Cas9, which is supported by that mCherry fluorescence also decreased with time in the control group. Thus, it is more reliable to interpret that the transfected plasmids were gradually degraded as time passed by.

After electroporation, we monitored the relative EGFP fluorescence every day and normalized each fluorescence signal to the value on Day 2 (see methods). In the control group, we observed that both green and red fluorescence signals were detected for 20 days as expected (Fig. 2B). In contrast, it is notable that green fluorescence started to decrease within a few days after the electroporation and almost disappeared on Day 20 in the CRISPR-Cas9 components-transfected group, while the red fluorescence persisted (Fig. 2B and S2A), suggesting that the endogenous EGFP gene was completely disrupted. One potential concern about this argument is that the decrease in EGFP fluorescence could be due to cell death. To address this, we further examined the morphology of the cells because cell death can be easily determined by the loss of soma and the fragmentized dendrites. By adjusting the contrast of the image to enhance the weakened mCherry signal, we could discriminate dead cells exhibiting the impaired morphology both

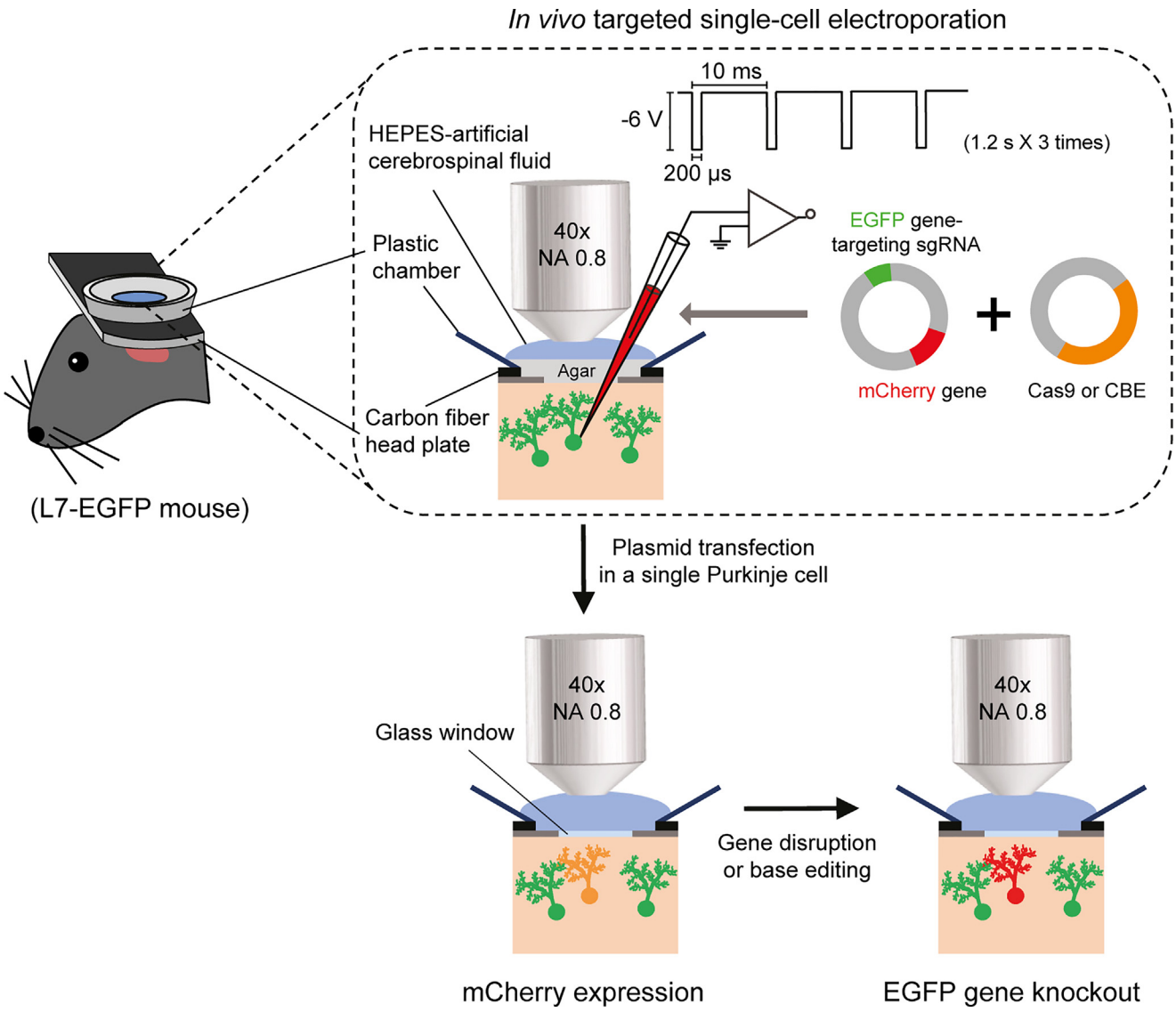

Fig. 1. Schematic illustration of *in vivo* gene knockout in a single cell. Two kinds of plasmid, respectively, coding Cas9 or CBE and sgRNA which targets an EGFP gene were prepared and electroporated into a target cell for EGFP gene knockout. The gene knockout was confirmed by monitoring the change of EGFP fluorescence after electroporation.

in soma and dendrites, thus we excluded those cells for further analysis (Fig. S3). Taken together, we concluded that the disappearance of EGFP fluorescence was not caused by cell death but by Cas9-mediated gene disruption.

In total, 8 of 10 Purkinje cells electroporated with the dual plasmids encoding CRISPR-Cas9 components showed obvious fade away of EGFP fluorescence throughout 3 weeks (defined as success) (1 of the 8 Purkinje cells was excluded in subsequent analyses because the monitoring EGFP fluorescence was disturbed by bleeding in the brain surface for the initial few days after electroporation) whereas EGFP fluorescence remained up to Day 20 in the other two Purkinje cells (defined as failure) (Fig. 2C). The higher success rate (80%) of this experiment than the out-of-frame rates (56.6% in Fig. S1C) calculated from *in vitro* experiment induced by Cas9/sgRNA#4, probably indicating that small changes including in-frame mutations of amino acid sequence in the functional domain could turn off the EGFP fluorescence [32,33]. In addition, we found that mCherry fluorescence observed on Day 5 in the failure group was relatively lower compared to the success group, suggesting that the failure of EGFP gene knockout might be due to insufficient delivery of the plasmids during the electroporation (Fig. S2B). In the 7 Purkinje cells of the success group, we obtained the average value of relative EGFP fluorescence signals per date and confirmed the gradual decrease of it compared to the negative control group (Fig. 2D), suggesting that it might take time that pre-existing EGFP mRNAs and proteins are degraded. We calculated the half-life of the EGFP fluorescence in each Purkinje cell by fitting the EGFP fluorescence to a single exponential decay function (Fig. S4), and the average half-life was 6.6 ± 0.8 days (n = 7).

3.3. CBE-mediated endogenous EGFP knockout in a single Purkinje cell

We next performed *in vivo* EGFP gene knockout experiments in a single cell through CBEs. Because the sgRNA#5 target sequences included two 5′-CAG-3′ sequences, encoding Gln at 184th and 185th amino acids respectively, we expected that the direct conversion of cytosine to thymine through CBEs could generate a premature termination codon (PTC), resulting in EGFP gene disruption [34,35] (Fig. 3A). To this end, we employed AncBE4max, an optimized CBE variant. With a positive confidence from the activity test in a human cell system (33.40% of C-to-T conversion rate generating TAG stop codon, Fig. S5), we electroporated the CBE components-encoding dual plasmids (i.e., one for CBE and the other for sgRNA#5/mCherry) into Purkinje cells *in vivo*, similar to

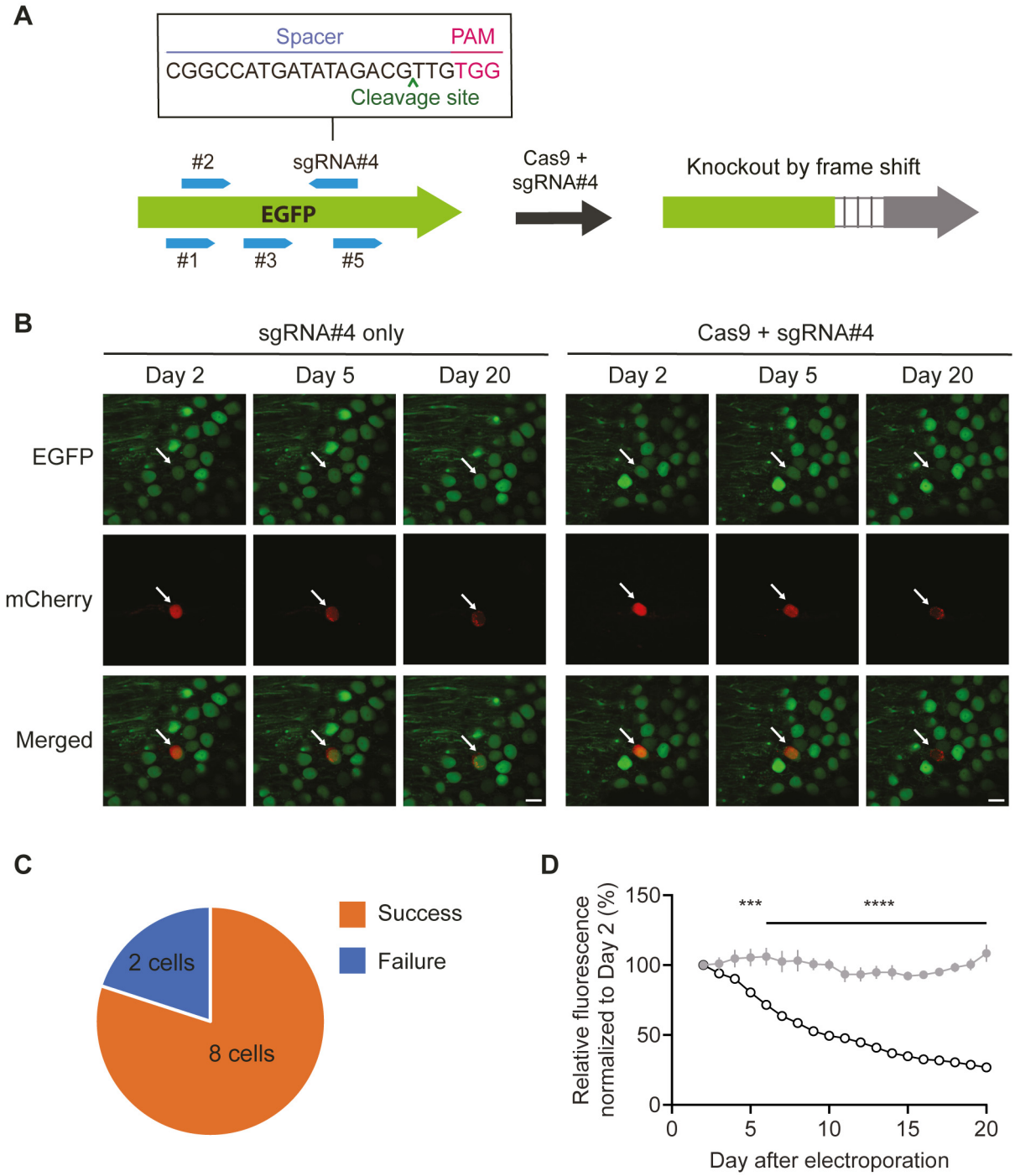

Fig. 2. Demonstration of *in vivo* gene knockout in a single cell by targeted single-cell electroporation combined with CRISPR/Cas9. (A) Illustration of EGFP gene knockout by CRISPR-Cas9. (B) Representative images showing that EGFP fluorescence in a Purkinje cell of an L7-EGFP mouse gradually decreased after electroporation of the dual plasmids encoding CRISPR-Cas9 components while it did not change in a Purkinje cell electroporated with sgRNA#4. White arrows indicate the electroporated cells. Scale bars, 20 μm. (C) A fraction of the Purkinje cells in which EGFP gene was knocked out by electroporation of the dual plasmids encoding CRISPR-Cas9 components. (D) A significant decrease of EGFP signals in the Purkinje cells electroporated with the dual plasmids encoding CRISPR-Cas9 components compared to the control group was observed 5 days after electroporation (filled circle, sgRNA#4, n = 6; open circle, Cas9 + sgRNA#4, n = 7; two-way ANOVA followed by *post hoc* Sidak's multiple comparison, Plasmid $F(1, 209) = 1331$, $p < 0.0001$; Time $F(18, 209) = 22.91$, $p < 0.0001$; Interaction $F(18, 209) = 15.74$, $p < 0.0001$). Error bars represent s.e.m.

the above Cas9 experiments. As a negative control, we transfected the sgRNA#5/mCherry-encoding plasmid alone.

In this experiment, we electroporated 68 Purkinje cells in 12 mice, and about half of them (38 cells, 56%) showed mCherry expression. Among the 38 mCherry-expressing cells, 22 cells (14 cells, CBE + sgRNA#5; 8 cells, sgRNA#5) survived throughout the experiment (for 3 weeks) (2 cells electroporated with sgRNA#5-encoding plasmid only were excluded in subsequent analyses due to the optical problem). Similar to the above results using Cas9 nucleases, Purkinje cells electroporated with the dual CBE components-encoding plasmids showed a gradual decrease in EGFP fluorescence, whereas there was no change in EGFP fluorescence in the Purkinje cells in the control group (Fig. 3B).

Among the 14 Purkinje cells which survived for three weeks after electroporation with the dual CBE components-encoding plasmids, 5 Purkinje cells showed the disappearance of EGFP fluo-

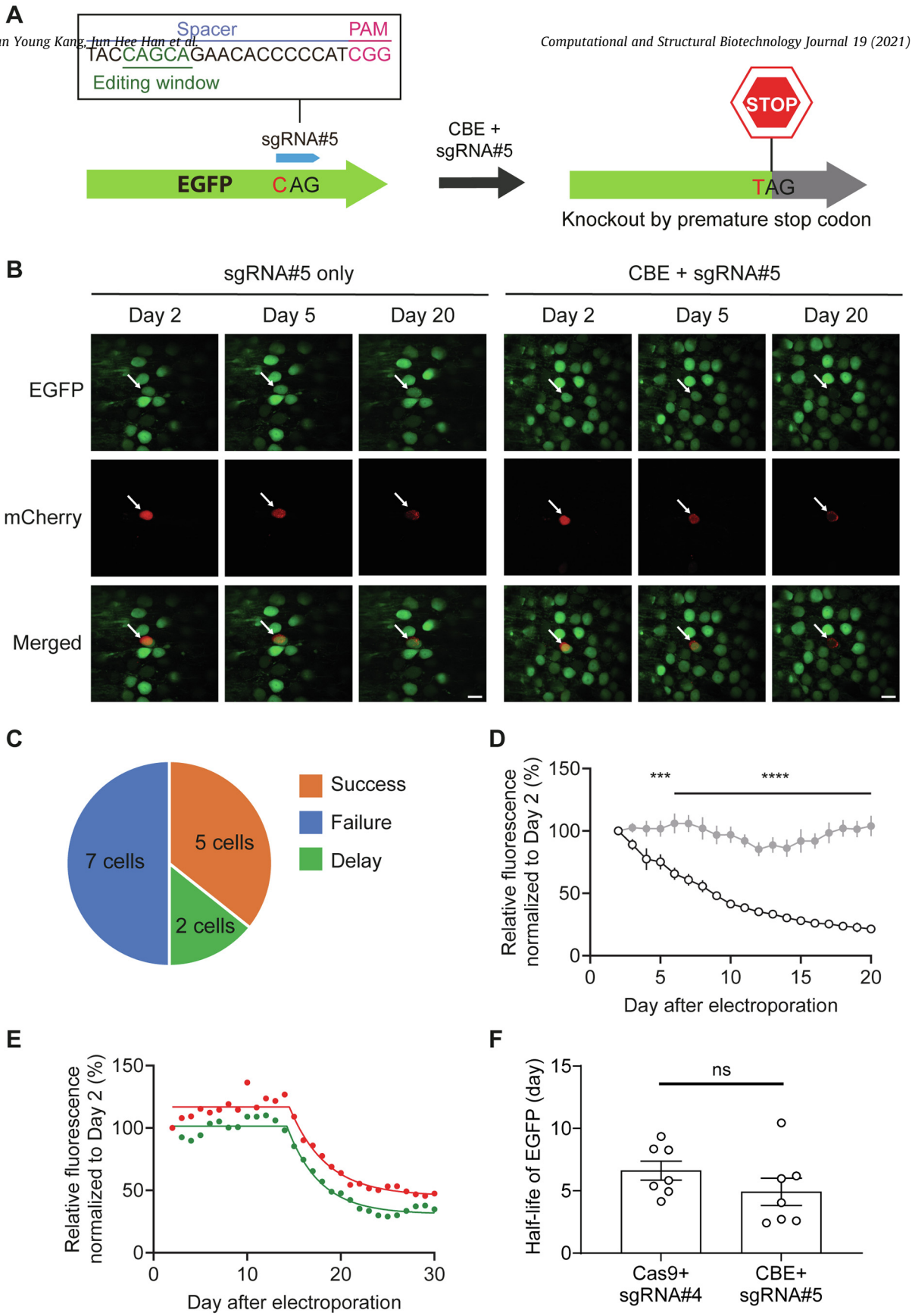

Fig. 3. Demonstration of *in vivo* gene knockout in a single cell by targeted single-cell electroporation combined with CBE. (A) Illustration of EGFP gene knockout by CBE. (B) Representative images showing that EGFP fluorescence in a Purkinje cell of an L7-EGFP mouse gradually decreased after electroporation of the CBE components-encoding dual plasmids while it did not change in a Purkinje cell electroporated with sgRNA#5. White arrows indicate the electroporated cells. Scale bars, 20 μm. (C) A fraction of the Purkinje cells in which *EGFP* gene was knocked out by electroporation of the dual plasmids encoding CBE components. (D) A significant decrease of EGFP signals in the Purkinje cells electroporated with the dual plasmids encoding CBE components compared to the control group was observed 5 days after electroporation (filled circle, sgRNA#5, n = 6; open circle, CBE + sgRNA#5, n = 5; two-way ANOVA followed by *post hoc* Sidak's multiple comparison, Plasmid $F(1, 171) = 707.6$, $p < 0.0001$; Time $F(18, 171) = 11.35$, $p < 0.0001$; Interaction, $F(18, 171) = 7.272$, $p < 0.0001$). (E) Reduction of EGFP fluorescence by EGFP gene knock out was delayed in two Purkinje cells electroporated with the dual plasmids encoding CBE components. The change of the EGFP fluorescence is fit to a single exponential curve following plateau ($r^2 > 0.95$). (f) Comparison of time constants in EGFP fluorescence reduction between Purkinje cells electroporated with the dual plasmids encoding CRISPR-Cas9 components and the dual plasmids encoding CBE components, respectively. Error bars represent s.e.m.

rescence on Day 20 (defined as success), whereas EGFP fluorescence remained up to Day 20 in other 7 Purkinje cells (defined as failure) (Fig. 3C and S6A). Notably, we found that in the remained two Purkinje cells, the EGFP fluorescence began to decrease more than 10 days after electroporation (defined as delay) (Fig. 3E and S6B). Similar to the failure group in the Cas9 experiment, we supposed that a sufficient amount of the plasmids might not be delivered into the Purkinje cells during electroporation in the delay and the failure groups. To verify this, we tried to compare mCherry fluorescence on Day 5 of each group. Resultantly, we observed that the mCherry fluorescence was relatively weaker both in the delay and the failure groups compared to the success group (Fig. S7), strongly supporting our claim that a smaller amount of the plasmids was transfected in the failure and the delay groups.

In addition, we found that the failure rate was higher in the CBE-transfected cells (7/14 = 50%, Fig. 3C), compared to the Cas9-transfected cells (2/10 = 20%, Fig. 2C). Considering our *in vitro* experiments in which CBE transfection showed ~ 33% C-to-T conversion rate (Fig. S5) while Cas9 transfection showed an > 85% indel frequency (Fig. S1), these results might be due to the difference in the efficiency between Cas9 and CBE. The larger size of the CBE-encoding plasmid (8961 bp), compared to that of the Cas9-encoding plasmid (7383 bp) might also negatively affect the delivery into the Purkinje cells during electroporation, resulting in the lower efficiency in the CBE-mediated gene knockout.

For the success group, we obtained the average value of relative EGFP fluorescence signals per date and confirmed a gradual decrease compared to the negative control group (Fig. 3D). We also calculated the half-life of EGFP fluorescence decay by fitting the EGFP fluorescence change to a single exponential decay function in the normal five Purkinje cells and by fitting a single exponential decay following plateau for the delayed two Purkinje cells (Fig. 3E and S8). The average half-life of EGFP is 4.9 ± 1.1 days (n = 7), which is not significantly different from the value from the above Cas9 experiments ($p = 0.2275$, Student's *t*-test) (Fig. 3F), suggesting that the decay time of pre-existing mRNAs and proteins was not affected by the genome editing tools.

4. Discussion

In this study, we demonstrated knockout of an endogenous EGFP gene in Purkinje cells of L7-EGFP mice at the single-cell level by combining an *in vivo* targeted single-cell electroporation technique and genome editing tools including Cas9 nucleases and CBEs. We could pinpoint the transfected cells *in vivo* and monitored the cell death after transfection, by introducing an additional mCherry gene for a red fluorescence signal. Because it is very difficult to directly detect the gene editing outcome from genome sequences in a single cell, we instead verified the endogenous EGFP gene knockout by measuring the gradual decrease of EGFP fluorescence signals. However, when endogenous genes are targeted, there would be no relevant marker such as EGFP. The most direct way to confirm the gene editing would be conducting DNA or mRNA sequencing of targeted cells, which can be done in the slices through *post hoc* analysis [36–38].

The L7-EGFP mice used in our experiments were generated using pL7ΔAUG vectors [24], so that EGFP genes could be randomly incorporated not only into the target site (L7 gene via a homologous recombination method) but also into multiple sites in the genome. The existence of multiple EGFP gene copies might also be related to the failure or the delay of gene knockout, in addition to the insufficient amounts of the genome editing tools estimated by comparing the mCherry fluorescence. Nevertheless, complete knockout of the multiple EGFP gene copies could be achieved by our method, thanks to the prominent editing capability of the CRISPR-Cas system. To quantify the exact copy number of EGFP genes or to identify the integrated region of EGFP genes in L7-EGFP mice, whole genome analysis using long-read sequencing platforms such as a nanopore sequencing [39,40] would be necessary.

By targeting EGFP genes in the genome of the L7-EGFP mice, we measured the *in vivo* half-life of EGFP (about 4.9 ~ 6.6 days) in Purkinje neurons of a living mouse after endogenous gene disruption via Cas9 nucleases or CBEs. Previously, several studies reported the half-life of EGFP in various cell types; >96 hrs in mouse embryonic stem cells [41], a few days in mouse neurons [42], and ~ 4.6 days in *Drosophila* S2 cells [43]. Because the half-life of EGFP largely varied depending on cell types and experimental surroundings, it is not easy to directly compare our results with the results in previous studies. Nevertheless, the half-life of EGFP in our experiments was somewhat longer than the previous results except the one measured in the *Drosophila* S2 cells, and this may be because there are multiple EGFP gene copies in the genome of L7-EGFP mice in our case. Therefore, endogenous genes as a single copy would be more suitable for analyzing the half-life of their products. Collectively, similar to measuring the half-life of EGFP protein in the success group in which EGFP gene was successfully knocked out, our method can be applied as a sensor for detecting the *in vivo* lifespan of the bio-molecules which may be different depending on different amounts of mRNA/protein levels and various degradation pathways.

On the other hand, because our study lacks functional analysis of the electroporated Purkinje cells, we could not rule out the possibility that neuronal activities changed due to the electroporation or the gene editing tools. However, the single-cell electroporation method is being widely used in neuroscience field to investigate neuronal function at a single-cell level, and there are several studies reporting that electroporation does not affect neuronal activities [44,45]. Given the previous studies, we thought that the possibilities of DNA-damage or of transfection-induced functional changes were very low. In addition, comparable levels of cell death during the experiment were observed in all the groups, suggesting that there was no apparent toxicity of Cas9 or CBE in our condition. However, in-depth studies revealing whether neuronal activities can be affected by the genome editing tools would be required in the future.

To date, several groups have carried out an *in vivo* targeted single-cell electroporation mainly for labeling cells [45–51] and for overexpressing specific genes [52–60], but regulating/engineering endogenous gene in a single neuron has not yet been demonstrated. To the best of our knowledge, the present research is the first demonstration of Cas9-mediated gene editing and CBE-mediated base editing in a single cell *in vivo*. The gene editing in a single-cell level is expected to enable more accurate gene function analysis in neural network. Because neurons are interconnected in various ways, gene editing at the population level can make the interpretation of the results from the gene modification complicated. In contrast, gene editing in a single-cell level can reveal gene function more accurately and directly. For example, with single-cell level gene editing, it is possible to study gene function within an individual by comparing the gene-edited neurons with non-edited ones, which can minimize the effect of differences among entities especially when the study is combined with a behavioral task such as learning or training. Neurons are the structural and functional units comprising the neural circuit in the brain, and the importance of research on neurons at a single-cell level is growing as much evidence is reported that a small number of neurons or even a single neuron is enough for inducing behavioral changes [61,62]. Therefore, our single-sell genome editing method would be highly useful in investigating the function of the brain with a fine resolution.

Although we demonstrated a single-gene knockout in the present study, we expect that multiple genes can be targeted simultaneously in a single cell, thanks to the multiplexing ability of CRISPR editing tools, by simply adding guide RNAs [63]. Moreover, in addition to Cas9 and CBEs demonstrated in this study, other CRISPR-associated tools such as CRISPRi for temporal gene inhibition [64], CRISPRa [65,66] for temporal gene activation, ABE [21] for adenine base editing, RNA editing/targeting [67,68], CRISPR-based chromatin remodeling [69,70], and the recently developed prime editing technology [71] can be adapted to our method. Taken together, our present study shows a simple and efficient way to manipulate a gene at the single-cell level *in vivo*, which is expected to evolve into various useful applications in the future.

Author contributions

S.B and B.S. conceived this project; B.S. performed *in vivo* gene editing experiments; C.Y.K. and J.H.H. prepared gene editing tools and performed *in vitro* experiments; B.S., C.Y.K., M.K., A.K., and S. B. analyzed the data; B.S., C.Y.K., and S.B. wrote the manuscript with input from all authors.

Declaration of Competing Interest

The authors declare that they have no known competing financial interests or personal relationships that could have appeared to influence the work reported in this paper.

Acknowledgments

We thank C. Yokoyama for proofreading the manuscript. This research was supported by grants from the National Research Foundation of Korea (NRF) (no. 2020M3A9I4036072 and no. 2021R1A2C3012908 to S.B.), by World Premier International Research Center Initiative (WPI, MEXT, Japan) (to A.K.), and by Grant-in-Aid for Scientific Research (18H04012 to M.K.) from the Japan Society for the Promotion of Science (JSPS).

Appendix A. Supplementary data

Supplementary data to this article can be found online at https://doi.org/10.1016/j.csbj.2021.04.051.

References

[1] Capecchi MR. The new mouse genetics: altering the genome by gene targeting. Trends Genet 1989;5(3):70–6.
[2] Koller BH, Smithies O. Altering genes in animals by gene targeting. Annu Rev Immunol 1992;10:705–30.
[3] Thomas KR, Capecchi MR. Site-directed mutagenesis by gene targeting in mouse embryo-derived stem cells. Cell 1987;51(3):503–12.
[4] Gu H, Marth JD, Orban PC, Mossmann H, Rajewsky K. Deletion of a DNA polymerase beta gene segment in T cells using cell type-specific gene targeting. Science 1994;265(5168):103–6.
[5] Kühn R, Schwenk F. Conditional knockout mice. Methods Mol Biol 2003;209:159–85.
[6] Kühn R, Schwenk F, Aguet M, Rajewsky K. Inducible gene targeting in mice. Science 1995;269(5229):1427–9.
[7] Garcia EL, Mills AA. Getting around lethality with inducible Cre-mediated excision. Semin Cell Dev Biol 2002;13(2):151–8.
[8] Lewandoski M. Conditional control of gene expression in the mouse. Nat Rev Genet 2001;2(10):743–55.
[9] Jinek M, Chylinski K, Fonfara I, Hauer M, Doudna JA, Charpentier E. A programmable dual-RNA-guided DNA endonuclease in adaptive bacterial immunity. Science 2012;337(6096):816–21.
[10] Wang H, Yang H, Shivalila CS, Dawlaty MM, Cheng AW, Zhang F, et al. One-step generation of mice carrying mutations in multiple genes by CRISPR/Cas-mediated genome engineering. Cell 2013;153(4):910–8.
[11] Cho SW, Kim S, Kim JM, Kim JS. Targeted genome engineering in human cells with the Cas9 RNA-guided endonuclease. Nat Biotechnol 2013;31(3):230–2.
[12] Chow RD, Guzman CD, Wang G, Schmidt F, Youngblood MW, Ye L, et al. AAV-mediated direct in vivo CRISPR screen identifies functional suppressors in glioblastoma. Nat Neurosci 2017;20(10):1329–41.
[13] Zheng Y, Shen W, Zhang J, Yang B, Liu YN, Qi H, et al. CRISPR interference-based specific and efficient gene inactivation in the brain. Nat Neurosci 2018;21(3):447–54.
[14] Sun H, Fu S, Cui S, Yin X, Sun X, Qi X, et al. Development of a CRISPR-SaCas9 system for projection- and function-specific gene editing in the rat brain. Sci Adv 2020;6(12):eaay6687.
[15] Swiech L, Heidenreich M, Banerjee A, Habib N, Li Y, Trombetta J, et al. In vivo interrogation of gene function in the mammalian brain using CRISPR-Cas9. Nat Biotechnol 2015;33(1):102–6.
[16] Monteys AM, Ebanks SA, Keiser MS, Davidson BL. CRISPR/Cas9 editing of the mutant huntingtin Allele in vitro and in vivo. Mol Ther 2017;25(1):12–23.
[17] Murlidharan G, Sakamoto K, Rao L, Corriher T, Wang D, Gao G, et al. CNS-restricted transduction and CRISPR/Cas9-mediated gene deletion with an engineered AAV vector. Mol Ther Nucleic Acids 2016;5(7):e338.
[18] Li Y, Kim J. Distinct roles of neuronal and microglial CB2 cannabinoid receptors in the mouse hippocampus. Neuroscience 2017;363:11–25.
[19] Komor AC, Kim YB, Packer MS, Zuris JA, Liu DR. Programmable editing of a target base in genomic DNA without double-stranded DNA cleavage. Nature 2016;533(7603):420–4.
[20] Nishida K, Arazoe T, Yachie N, Banno S, Kakimoto M, Tabata M, et al. Targeted nucleotide editing using hybrid prokaryotic and vertebrate adaptive immune systems. Science 2016;353(6305).
[21] Gaudelli NM, Komor AC, Rees HA, Packer MS, Badran AH, Bryson DI, et al. Programmable base editing of A*T to G*C in genomic DNA without DNA cleavage. Nature 2017;551(7681):464–71.
[22] Kitamura K, Judkewitz B, Kano M, Denk W, Hausser M. Targeted patch-clamp recordings and single-cell electroporation of unlabeled neurons in vivo. Nat Methods 2008;5(1):61–7.
[23] Judkewitz B, Rizzi M, Kitamura K, Hausser M. Targeted single-cell electroporation of mammalian neurons in vivo. Nat Protoc 2009;4(6):862–9.
[24] Uesaka N, Uchigashima M, Mikuni T, Nakazawa T, Nakao H, Hirai H, et al. Retrograde semaphorin signaling regulates synapse elimination in the developing mouse brain. Science 2014;344(6187):1020–3.
[25] Park J, Bae S, Kim JS. Cas-Designer: a web-based tool for choice of CRISPR-Cas9 target sites. Bioinformatics 2015;31(24):4014–6.
[26] Park J, Lim K, Kim JS, Bae S. Cas-analyzer: an online tool for assessing genome editing results using NGS data. Bioinformatics 2017;33(2):286–8.
[27] Hwang GH, Park J, Lim K, Kim S, Yu J, Yu E, et al. Web-based design and analysis tools for CRISPR base editing. BMC Bioinf 2018;19(1):542.
[28] Jeong YK, Yu J, Bae S. Construction of non-canonical PAM-targeting adenosine base editors by restriction enzyme-free DNA cloning using CRISPR-Cas9. Sci Rep 2019;9(1):4939.
[29] Chen B, Gilbert LA, Cimini BA, Schnitzbauer J, Zhang W, Li GW, et al. Dynamic imaging of genomic loci in living human cells by an optimized CRISPR/Cas system. Cell 2013;155(7):1479–91.
[30] Chen X, Leischner U, Varga Z, Jia H, Deca D, Rochefort NL, et al. LOTOS-based two-photon calcium imaging of dendritic spines in vivo. Nat Protoc 2012;7(10):1818–29.
[31] Schneider CA, Rasband WS, Eliceiri KW. NIH Image to ImageJ: 25 years of image analysis. Nat Methods 2012;9(7):671–5.
[32] Li X, Zhang G, Ngo N, Zhao X, Kain SR, Huang CC. Deletions of the Aequorea victoria green fluorescent protein define the minimal domain required for fluorescence. J Biol Chem 1997;272(45):28545–9.
[33] Dopf J, Horiagon TM. Deletion mapping of the Aequorea victoria green fluorescent protein. Gene 1996;173(1 Spec No):39–44.
[34] Billon P, Bryant EE, Joseph SA, Nambiar TS, Hayward SB, Rothstein R, et al. CRISPR-mediated base editing enables efficient disruption of eukaryotic genes through induction of STOP codons. Mol Cell 2017;67(6):1068–1079 e1064.
[35] Kuscu C, Parlak M, Tufan T, Yang J, Szlachta K, Wei X, et al. CRISPR-STOP: gene silencing through base-editing-induced nonsense mutations. Nat Methods 2017;14(7):710–2.
[36] Garaschuk O, Schneggenburger R, Schirra C, Tempia F, Konnerth A. Fractional Ca2+ currents through somatic and dendritic glutamate receptor channels of rat hippocampal CA1 pyramidal neurones. J Physiol 1996;491(Pt 3):757–72.
[37] Plant TD, Schirra C, Katz E, Uchitel OD, Konnerth A. Single-cell RT-PCR and functional characterization of Ca2+ channels in motoneurons of the rat facial nucleus. J Neurosci 1998;18(23):9573–84.
[38] Steinecke A, Kurabayashi N, Hayano Y, Ishino Y, Taniguchi H. In vivo single-cell genotyping of mouse cortical neurons transfected with CRISPR/Cas9. Cell Rep 2019;28(2):325–331 e324.
[39] Branton D, Deamer DW, Marziali A, Bayley H, Benner SA, Butler T, et al. The potential and challenges of nanopore sequencing. Nat Biotechnol 2008;26(10):1146–53.
[40] Jain M, Olsen HE, Paten B, Akeson M. The Oxford Nanopore MinION: delivery of nanopore sequencing to the genomics community. Genome Biol 2016;17(1):239.
[41] Nakai-Futatsugi Y, Niwa H. Zscan4 is activated after telomere shortening in mouse embryonic stem cells. Stem Cell Rep 2016;6(4):483–95.
[42] Schubert S, Moller-Ehrlich K, Singethan K, Wiese S, Duprex WP, Rima BK, et al. A mouse model of persistent brain infection with recombinant Measles virus. J Gen Virol 2006;87(Pt 7):2011–9.

[43] Verkhusha VV, Kuznetsova IM, Stepanenko OV, Zaraisky AG, Shavlovsky MM, Turoverov KK, et al. High stability of Discosoma DsRed as compared to Aequorea EGFP. Biochemistry 2003;42(26):7879–84.
[44] Rathenberg J, Nevian T, Witzemann V. High-efficiency transfection of individual neurons using modified electrophysiology techniques. J Neurosci Methods 2003;126(1):91–8.
[45] Cohen L, Koffman N, Meiri H, Yarom Y, Lampl I, Mizrahi A. Time-lapse electrical recordings of single neurons from the mouse neocortex. Proc Natl Acad Sci U S A 2013;110(14):5665–70.
[46] Andrasfalvy BK, Galinanes GL, Huber D, Barbic M, Macklin JJ, Susumu K, et al. Quantum dot-based multiphoton fluorescent pipettes for targeted neuronal electrophysiology. Nat Methods 2014;11(12):1237–41.
[47] Yamashita T, Pala A, Pedrido L, Kremer Y, Welker E, Petersen CC. Membrane potential dynamics of neocortical projection neurons driving target-specific signals. Neuron 2013;80(6):1477–90.
[48] Yamashita T, Vavladeli A, Pala A, Galan K, Crochet S, Petersen SSA, et al. Diverse long-range axonal projections of excitatory layer 2/3 neurons in mouse barrel cortex. Front Neuroanat 2018;12:33.
[49] Oyama K, Ohara S, Sato S, Karube F, Fujiyama F, Isomura Y, et al. Long-lasting single-neuron labeling by in vivo electroporation without microscopic guidance. J Neurosci Methods 2013;218(2):139–47.
[50] Long B, Li L, Knoblich U, Zeng H, Peng H. 3D image-guided automatic pipette positioning for single cell experiments in vivo. Sci Rep 2015;5:18426.
[51] Li L, Ouellette B, Stoy WA, Garren EJ, Daigle TL, Forest CR, et al. A robot for high yield electrophysiology and morphology of single neurons in vivo. Nat Commun 2017;8:15604.
[52] Pala A, Petersen CCH. In vivo measurement of cell-type-specific synaptic connectivity and synaptic transmission in layer 2/3 mouse barrel cortex. Neuron 2015;85(1):68–75.
[53] Rossi T, Gallerani G, Angeli D, Cocchi C, Bandini E, Fici P, et al. Single-cell NGS-based analysis of copy number alterations reveals new insights in circulating tumor cells persistence in early-stage breast cancer. Cancers (Basel) 2020;12(9).
[54] Pala A, Petersen CC. State-dependent cell-type-specific membrane potential dynamics and unitary synaptic inputs in awake mice. Elife 2018;7.
[55] Marshel JH, Mori T, Nielsen KJ, Callaway EM. Targeting single neuronal networks for gene expression and cell labeling in vivo. Neuron 2010;67(4):562–74.
[56] Rompani SB, Mullner FE, Wanner A, Zhang C, Roth CN, Yonehara K, et al. Different modes of visual integration in the lateral geniculate nucleus revealed by single-cell-initiated transsynaptic tracing. Neuron 2017;93(4):767–776 e766.
[57] Wertz A, Trenholm S, Yonehara K, Hillier D, Raics Z, Leinweber M, et al. Presynaptic networks. Single-cell-initiated monosynaptic tracing reveals layer-specific cortical network modules. Science 2015;349(6243):70–4.
[58] Cottam JC, Smith SL, Hausser M. Target-specific effects of somatostatin-expressing interneurons on neocortical visual processing. J Neurosci 2013;33(50):19567–78.
[59] El-Boustani S, Ip JPK, Breton-Provencher V, Knott GW, Okuno H, Bito H, et al. Locally coordinated synaptic plasticity of visual cortex neurons in vivo. Science 2018;360(6395):1349–54.
[60] Pagès S, Cane M, Randall J, Capello L, Holtmaat A. Single cell electroporation for longitudinal imaging of synaptic structure and function in the adult mouse neocortex in vivo. Front Neuroanat 2015;9:36.
[61] Li CY, Poo MM, Dan Y. Burst spiking of a single cortical neuron modifies global brain state. Science 2009;324(5927):643–6.
[62] Robinson NTM, Descamps LAL, Russell LE, Buchholz MO, Bicknell BA, Antonov GK, et al. Targeted activation of hippocampal place cells drives memory-guided spatial behavior. Cell 2020;183(7):2041–2.
[63] McCarty NS, Graham AE, Studena L, Ledesma-Amaro R. Multiplexed CRISPR technologies for gene editing and transcriptional regulation. Nat Commun 2020;11(1):1281.
[64] Qi LS, Larson MH, Gilbert LA, Doudna JA, Weissman JS, Arkin AP, et al. Repurposing CRISPR as an RNA-guided platform for sequence-specific control of gene expression. Cell 2013;152(5):1173–83.
[65] Maeder ML, Linder SJ, Cascio VM, Fu Y, Ho QH, Joung JK. CRISPR RNA-guided activation of endogenous human genes. Nat Methods 2013;10(10):977–9.
[66] Perez-Pinera P, Kocak DD, Vockley CM, Adler AF, Kabadi AM, Polstein LR, et al. RNA-guided gene activation by CRISPR-Cas9-based transcription factors. Nat Methods 2013;10(10):973–6.
[67] Cox DBT, Gootenberg JS, Abudayyeh OO, Franklin B, Kellner MJ, Joung J, et al. RNA editing with CRISPR-Cas13. Science 2017;358(6366):1019–27.
[68] Abudayyeh OO, Gootenberg JS, Essletzbichler P, Han S, Joung J, Belanto JJ, et al. RNA targeting with CRISPR-Cas13. Nature 2017;550(7675):280–4.
[69] Black JB, Adler AF, Wang HG, D'Ippolito AM, Hutchinson HA, Reddy TE, et al. Targeted epigenetic remodeling of endogenous loci by CRISPR/Cas9-based transcriptional activators directly converts fibroblasts to neuronal cells. Cell Stem Cell 2016;19(3):406–14.
[70] Chakraborty S, Ji H, Kabadi AM, Gersbach CA, Christoforou N, Leong KW. A CRISPR/Cas9-based system for reprogramming cell lineage specification. Stem Cell Rep 2014;3(6):940–7.
[71] Anzalone AV, Randolph PB, Davis JR, Sousa AA, Koblan LW, Levy JM, et al. Search-and-replace genome editing without double-strand breaks or donor DNA. Nature 2019;576(7785):149–57.